Cite This: ACS Energy Lett. 2018, 3, 961−969

ACS Energy

[redacted]sition on Photoanodes: The Roles of Intrinsic Catalytic Activity, Catalyst Electrical Conductivity, and Semiconductor Morphology

Jingjing Qiu,[†] Hamed Hajibabaei,[‡] Michael R. Nellist,[†] Forrest A. L. Laskowski,[†] Sebastian Z. Oener,[†] Thomas W. Hamann,[‡] and Shannon W. Boettcher*[,†]

[†] Department of Chemistry and Biochemistry, Materials Science Institute, University of Oregon, Eugene, Oregon 97403, United States

[‡] Department of Chemistry, Michigan State University, East Lansing, Michigan 48824, United States

* Supporting Information

ABSTRACT: Semiconducting oxide photoanodes are used to drive the oxygen evolution reaction (OER) in water-splitting systems. The highest-performing systems use nanostructured semiconductors coated with water-oxidation catalysts. Despite much work, the design principles governing the integration of catalysts with semiconductors are poorly understood. Using hematite as a model system, we show how semiconductor morphology and electrical conductivity of the catalyst affect the system photoresponse. Electrically conductive catalysts can introduce substantial "shunt" recombination currents if they contact both the semiconductor surface and the underlying conducting-glass substrate, leading to poor performance. This recombination can be largely eliminated by using pinhole-free semiconductors, using selective photoassisted electrodeposition of thin catalyst layers on the semiconductor surface, using electrically insulating catalyst layers, or adding an intermediate insulating oxide layer. The results of this study are used to clarify the mechanisms behind several important results reported in the literature.

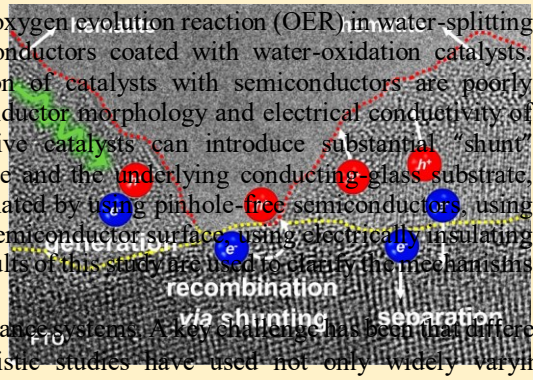

Photoelectrochemical (PEC) water splitting is one approach to generate fuels using solar energy.[1] In particular, much effort has been extended toward developing photoanodes to drive the oxygen evolution reaction (OER), which typically limits the overall efficiency of PEC water-splitting devices.[2] Particular emphasis has been placed on metal-oxide photoanodes, as they, in principle, can be thermodynamically stable under OER conditions.[3] Recent efforts have focused on synthesizing lower band gap oxide semiconductors to absorb more visible light;[4,5] nanostructuring photoanodes to improve carrier collection and increase photocurrent;[6−9] and adding electrocatalytic surface layers that increase the photovoltage, photocurrent, or both.[10−13]

Among these three efforts, the roles of electrocatalytic layers in improving performance are the most poorly understood,[14] despite the fact that optimizing the semiconductor|electrocatalyst (sem|cat) interface is critical for designing high-performance systems.[15−17] A key challenge has been that different mechanistic studies have used not only widely varying characterization techniques but also a wide range of semiconductor and electrocatalyst morphologies and properties.

Much work in this area has focused on hematite, where the deposition of an electrocatalyst layer generally leads to a cathodic shift in the photocurrent onset potential as well as an increase in the photocurrent, especially at lower applied potentials.[10,11,18] For example, Wang and co-workers reported a dramatic enhancement of photocurrent and photovoltage by spin-coating $NiFeO_x$ onto hematite thin films.[19,20] They conclude, on the basis of fits to intensity-modulated photocurrent spectroscopy (IMPS) data, that $NiFeO_x$ passivates the surface but does not catalyze the reaction.[21] Using IMPS, van de Krol and co-workers also proposed that electrodeposited cobalt (oxy)hydroxide phosphate (CoPi) reduces surface recombination of $BiVO_4$.[22] Transient absorption spectroscopy (TAS) results have

DOI: 10.1021/acsenergylett.8b00336
ACS Energy Lett. 2018, 3, 961−969

further been interpreted to conclude that CoPi primarily altered the band bending of mesostructured hematite (α-Fe_2O_3).[23] In contrast to the proposed passivating effects of some catalyst layers, in situ X-ray absorption studies

Received: February 28, 2018
Accepted: March 20, 2018
Published: March 20, 2018

electron transfer throughout the system. We have extended this method to the nanoscale, using potential-sensing electrochemical atomic-force microscopy to monitor hole accumulation on electrodeposited CoPi from illuminated hematite.[27] It was shown that CoPi accumulates holes and reaches an electrochemical potential sufficient to drive water oxidation at the photocurrent density.[27]

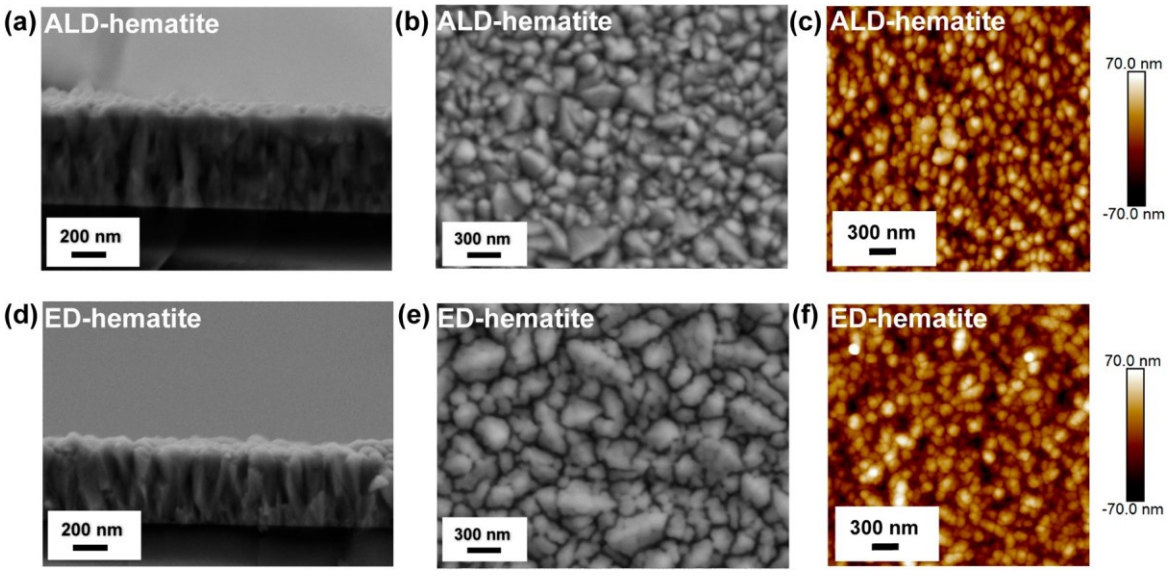

Figure 1. Scanning electron microscopy (SEM) and atomic force microscopy (AFM) images of (a−c) ALD-hematite and (d−f) ED-hematite thin films.

of MnO_x-coated $BiVO_4$ show that the Mn metal center is oxidized when the semiconductor is illuminated, indicating photogenerated hole transfer from the semiconductor to the catalyst layer. Quantitative knowledge of the hole-transfer efficiency, however, is unknown.[25]

Gamelin and co-workers studied CoPi on mesostructured hematite consisting of a highly structured surface with resolvable features on the order of ~10 nm in diameter.[12] They observe that CoPi improves the performance of mesostructured hematite only when thin layers were used; thicker layers (~25 nm) led to worse performance, which they attribute to increased interfacial recombination between conduction band electrons traversing the nanostructured semiconductor to the back contact and holes accumulated in the thicker layer of CoPi.[12] Impedance-based studies have similarly found the CoPi is charged by holes from hematite and that even thick CoPi films (~400 nm) enhance the PEC performance when the catalyst is deposited on pinhole-free hematite films made by atomic-layer deposition (ALD).[24]

We have recently demonstrated that $Ni_{0.8}Fe_{0.2}O_xH_y$ films deposited on α-Fe_2O_3 (fabricated by ALD) act as both holecollecting contacts and catalysts for water oxidation based on direct in situ measurements of the sem|cat interfacial currents and catalyst potential using a dual-working-electrode (DWE) technique.[18,26] The DWE technique is useful in that it can be used to directly measure

Conflicting results have also been observed for seemingly similar systems. Young et al. showed that Ni (oxy)hydroxide improves the efficiency of hematite thin films prepared via ALD,[28] but Li and co-workers observed that Ni (oxy)hydroxide-functionalized hematite nanowire arrays have a lower steady-state photocurrent than bare hematite nanowires.[29] When the loading of Ni (oxy)hydroxide is decreased, Ni (oxy)hydroxide-functionalized hematite nanowires show slightly increased photocurrents.[29] Morphology differences in the hematite may play a role in the different observed behaviors of the electrocatalyst, a point we will examine below.

The composition of the catalyst itself also appears to affect the measured response. Hamann and co-workers investigated how the ratio of Ni and Fe in a $Ni(Fe)O_xH_y$ catalyst affects the photoresponse of hematite photoanodes. They observed that Ni-rich $Ni_{0.75}Fe_{0.25}O_xH_y$ electrocatalyst films inhibit the PEC performance of electrodeposited hematite, but Fe-rich $Ni_{0.25}Fe_{0.75}O_xH_y$ does not.[30] This was surprising, as the Nirich phases are known to be better OER electrocatalysts.[31] They attributed this difference to interface trap states formed between Ni-rich catalyst and electrodeposited hematite.[30] Choi and co-workers found that when electrodeposited nanoporous $BiVO_4$ is interfaced with FeOOH and NiOOH "bilayer" catalysts, the PEC performance is much better than when NiOOH alone is used.

DOI: 10.1021/acsenergylett.8b00336
ACS Energy Lett. 2018, 3, 961−969

The improvement is attributed to reduced interfacial recombination with FeOOH.[32]

The above results demonstrate a wide range of experimental observations and mechanistic interpretations. Here we attempt to unify some of the disparate interpretations by showing how semiconductor morphology (specifically accounting for incomplete coverage of the underlying conducting glass substrate) and electrical conductivity of the catalyst (which can be systematically controlled via composition) affect the system photoresponse. While we focus on hematite as a model oxide photoanode material, the results have implications for other material systems. We compare hematite thin films deposited on fluorinated tin oxide (FTO)-glass by ALD with those from electrodeposition. While the film morphology and roughness of ALD-hematite and electrodeposited (ED) hematite appear nearly identical in SEM and AFM imaging (Figure 1), crosssectional transmission electron microscopy (TEM) imaging reveals that ED-hematite incompletely covers the FTO surface (i.e., there are pinholes). We then interface the ALD and ED hematite with Ni(Fe) oxyhydroxide catalysts synthesized by different methods. We choose Ni(Fe) oxyhydroxide as a catalyst because it (1) is among the most active electrocatalysts for water oxidation,[31] (2) has an intrinsic catalyst activity that can be tuned by Fe content,[33−37] and (3) exhibits an electrical conductivity that depends on Fe content.[31,33] We then study the sem|cat interface via dual-electrode voltammetry (shown in Scheme S1), using the second working electrode to contact the catalyst layer and directly measure voltage/current.

Our measurements show that when porous ED hematite is interfaced with electrically conductive catalysts, such as $Ni_{0.8}Fe_{0.2}O_xH_y$, severe recombination can occur via direct shunting to the underlying FTO. Sufficiently thick catalyst coating via electrodeposition or uniform deposition by spin coating promote this effect by creating conduction paths between the catalyst and the conductive substrate. Such recombination currents are not present for dense ALDdeposited hematite films that lack these shunt pathways. Devices made by the deposition of equivalently thick $Ni_{0.2}Fe_{0.8}O_xH_y$ on porous hematite also exhibit no shunting behavior, because the high Fe content makes the catalyst an electrical insulator.[38,39] Alternatively we find that photoassisted electrodeposition of Ni-rich Ni(Fe) (oxy)hydroxide on the (porous) ED-hematite can be used to improve its performance if the layers are kept sufficiently thin such that direct shunting to the conductive glass substrate is prevented. This result furthermore indicates that the shunts are not formed because of electromigration or intrinsic defect-assisted conduction under operation conditions but via the deposition of conductive catalyst onto or into the porous hematite film.

The Role of Electrocatalyst Electrical Conductivity in Photoelectrode Behavior. Smooth $Ni_xFe_{1-x}O_yH_z$ electrocatalyst films were spin-cast onto ALD-hematite and ED-hematite substrates using the photo metal−organic deposition (PMOD) method.[40] Two compositions, $Ni_{0.8}Fe_{0.2}O_xH_y$ and $Ni_{0.2}Fe_{0.8}O_xH_y$, were chosen to represent Ni- and Fe-rich catalysts. The electrocatalysts were also deposited on indium-tin-oxide (ITO) coated glass substrates to analyze their intrinsic catalytic properties. $Ni_{0.8}Fe_{0.2}O_xH_y$ is much more active than $Ni_{0.2}Fe_{0.8}O_xH_y$ as indicated by a more-cathodic onset of OER current (Figure 2a).[31] The $Ni(Fe)O_xH_y$ layer becomes conductive when the Ni cations are oxidized.[41] A low concentration of Fe (<25%) in NiOOH may improve the electrical conductivity,[31] but pure FeOOH is an insulator.[39] Here we find the electrical conductivity, measured in situ, of $Ni_{0.8}Fe_{0.2}O_xH_y$ is ~10^{-2} mS·cm^{-1} at 0.25

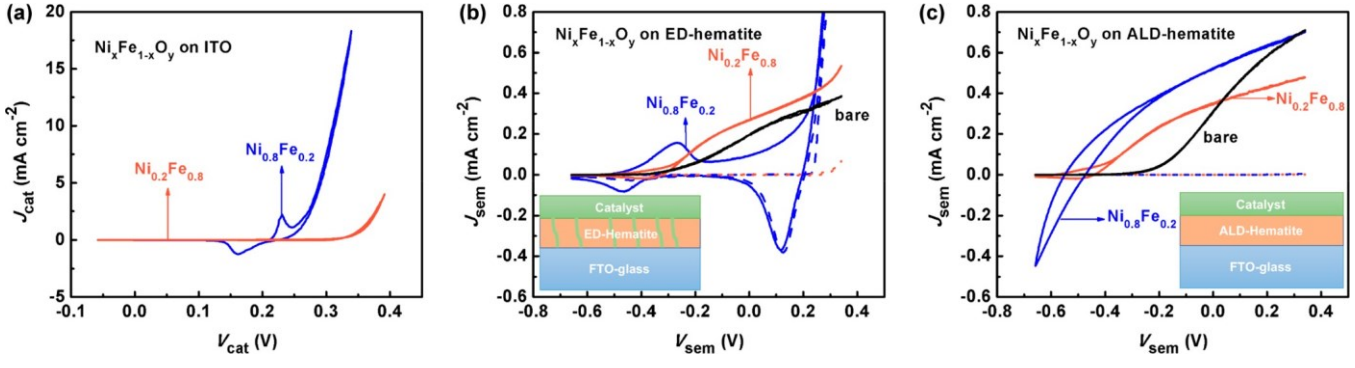

Figure 2. Voltammetry of $Ni_{0.8}Fe_{0.2}O_xH_y$ and $Ni_{0.2}Fe_{0.8}O_xH_y$ films and catalyst-coated ED hematite and ALD hematite electrodes. (a) Voltammograms of $Ni_{0.8}Fe_{0.2}O_xH_y$ and $Ni_{0.2}Fe_{0.8}O_xH_y$ films measured on ITO substrates. (b) Current−potential response in the light (solid lines) and dark (dotted lines) of $Ni_{0.8}Fe_{0.2}O_xH_y$ (blue) and $Ni_{0.2}Fe_{0.8}O_xH_y$ (orange) coated on ED hematite. (c) Current−potential response in the light (solid lines) and dark (dotted lines) of $Ni_{0.8}Fe_{0.2}O_xH_y$ (blue) and $Ni_{0.2}Fe_{0.8}O_xH_y$ (orange) coated on ALD hematite. The insets in panels b and c are schematics of the electrodes. The potentials V_{sem} and V_{cat} are reported versus ε_{O_2/OH^-}. All CVs were measured in 0.1 M KOH at a scan rate of 10 mV·s^{-1}. The semiconductor samples were illuminated from the FTO glass side with ~100 mW·cm^{-2} of AM1.5G solar simulation.

DOI: 10.1021/acsenergylett.8b00336
ACS Energy Lett. 2018, 3, 961−969

V vs ε_{O_2/OH^-} (measured in the DWE geometry).[18] This value is 5 orders of magnitude higher than that of the Fe-rich $Ni_{0.2}Fe_{0.8}O_xH_y$, which has a conductivity of ~10^{-7} mS·cm^{-1} after being oxidized at 0.35 V vs ε_{O_2/OH^-} (Figure S1). $Ni_{0.8}Fe_{0.2}O_xH_y$ also has a higher percentage of electrochemically accessible Ni cations than $Ni_{0.2}Fe_{0.8}O_xH_y$ of a similar thickness, as is apparent by the large redox wave (Figure 2a).

The more active catalyst ($Ni_{0.8}Fe_{0.2}O_xH_y$) and the less active one ($Ni_{0.2}Fe_{0.8}O_xH_y$) affected the PEC performance of ALDhematite and ED-hematite electrodes differently. The Fe-rich catalyst enhanced the performance of ED-hematite substantially, while the Ni-rich catalyst decreased the performance (Figure 2b). For the ALD-hematite, both catalysts improved its performance, although the higher-activity Ni-rich catalyst exhibited greater improvement than the Fe-rich one (Figure 2c).

The dark current−potential data (dashed lines in Figure 2) are different for catalyzed ED-hematite and ALD-hematite. For ALD-hematite electrodes with either catalyst, and for the $Ni_{0.2}Fe_{0.8}O_xH_y$-coated ED hematite, the dark currents are small over the whole voltage range, as shown in panels c and b of Figure 2, respectively. However, the dark current for $Ni_{0.8}Fe_{0.2}O_xH_y$-catalyzed ED-hematite is much larger than that of the $Ni_{0.8}Fe_{0.2}O_xH_y$-catalyzed ALD-hematite. Additionally, the reduction peak at ~0.16 V vs ε_{O_2/OH^-} (Figure 2b) occurs at the same potential as the reduction of $Ni_{0.8}Fe_{0.2}O_xH_y$ on ITO (Figure 2a). This data suggests direct contact between the catalyst and conducting FTO substrate for the ED-hematite sample, likely through pinholes. The fact that the ALDhematite does not show this behavior suggests that pinholes are not present in the ALD-hematite film.[42]

Illumination of the $Ni_{0.8}Fe_{0.2}O_xH_y$-catalyzed ED-hematite leads to a marginal increase in photocurrent as well as a new redox wave centered at −0.4 V vs ε_{O_2/OH^-} (Figure 2b). The fact that two redox waves are observed for the $Ni_{0.8}Fe_{0.2}O_xH_y$catalyzed ED-hematite suggests that the $Ni_{0.8}Fe_{0.2}O_xH_y$ catalyst is in two distinct environments: one in primary contact with the FTO substrate (reduction peak at ~0.16 V vs ε_{O_2/OH^-}) and the other in primary contact with the hematite (whose redox waves are shifted cathodic and centered at −0.4 V vs ε_{O_2/OH^-} because of the photovoltage generated by the hematite).

High-resolution transmission electron microscopy (HRTEM) cross-sectional imaging was used to confirm the presence of pinholes due to incomplete hematite coverage for the ED samples. Figure 3 shows that the ALD-hematite thin film is uniform and compact while the ED-hematite thin film is not. Direct contact between the catalyst layer and the underlying FTO is evident in Figure 3b.

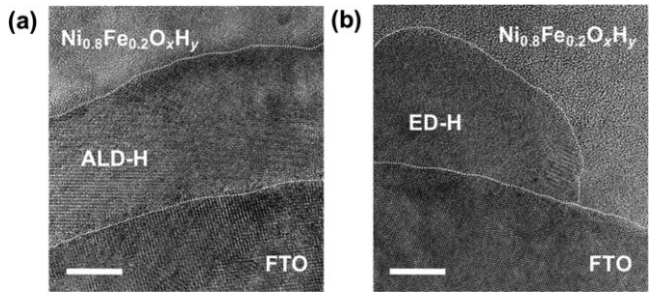

Figure 3. High-resolution TEM cross-sectional images of (a) ALDhematite|$Ni_{0.8}Fe_{0.2}O_xH_y$ and (b) ED-hematite|$Ni_{0.8}Fe_{0.2}O_xH_y$ interfaces. The scale bars are 10 nm. The white dashed lines mark the interfaces.

We next compared the voltammetry of bare FTO, EDhematite-coated FTO, and ALD-hematite-coated FTO in 10 mM aq $[Fe^{II}(CN)_6]^{4-}$ in the dark. While the ALD-hematite showed negligible current, consistent with the large energy barrier at the semiconductor|liquid junction, the response from the ED-hematite was similar to that of the bare FTO electrode (Figure S2). This data suggests the pinholes are prevalent in large number across the ED-hematite film.

The photoelectrochemical data in Figure 2 show that for $Ni_{0.8}Fe_{0.2}O_xH_y$-catalyzed ED-hematite the catalyst is not simply increasing OER kinetics but also dramatically increasing recombination. The recombination mechanism is not present when $Ni_{0.2}Fe_{0.8}O_xH_y$ is used as a catalyst (which is not electrically conductive, see Figure S1) nor when ALD-hematite is used as the semiconductor. A simple mechanism to explain this behavior would be recombination of the photogenerated holes through conductive paths associated with direct contact between $Ni_{0.8}Fe_{0.2}O_xH_y$ catalyst and FTO, i.e., a shunt.

Dual-Working-Electrode Measurements to Assess Recombination Paths. To test the hypothesis of shunting recombination across pinholes in the ED-hematite, we applied the DWE technique to monitor the potential/current of/across the semiconductor and catalyst layers in situ. Four types of devices were prepared to compare the impact of catalyst composition on different hematite samples: ED-hematite|$Ni_{0.8}Fe_{0.2}O_xH_y$|Au, ALD-hematite|$Ni_{0.8}Fe_{0.2}O_xH_y$|Au, ED-hematite|$Ni_{0.2}Fe_{0.8}O_xH_y$|Au, and ALD-hematite|$Ni_{0.2}Fe_{0.8}O_xH_y$|Au.

Scheme 1 shows a schematic band bending diagram of hematite in contact with an electrolyte-permeable electrocatalyst and a second Au working electrode (WE2) when V_{sem} is fixed at 0 V vs ε_{O_2/OH^-}. E_{sem}, E_{cat}, and E_{sol} represent the Fermi levels of the semiconductor (sem), catalyst layer

DOI: 10.1021/acsenergylett.8b00336
ACS Energy Lett. 2018, 3, 961−969

(cat), and solution (sol), respectively. J_e and J_h are electron and hole current densities through the semiconductor, and J_{cat} is the catalytic current density. Under illumination, the photogenerated holes on the surface of α-Fe_2O_3 transfer to the Ni(Fe)O_xH_y catalyst, which leads to Ni oxidation.[18] The oxidized $Ni_{0.8}Fe_{0.2}O_xH_y$ is electrically conductive, allowing its potential to be sensed via WE2, and the catalyst potential increases upon hole collection until the catalytic current (J_{cat}) matches the photocurrent ($J_{sem,light}$).[18] The direct measurement of catalyst potential (V_{WE2}) shows that $Ni_{0.8}Fe_{0.2}O_xH_y$ on EDhematite is charged to ~0.21 V vs ε_{O_2/OH^-} (Figure 4a, red points) while the potential of $Ni_{0.8}Fe_{0.2}O_xH_y$ on ALD-hematite reaches ~0.24 V vs ε_{O_2/OH^-} (Figure 4d, red points) when V_{sem} = 0.15 V vs ε_{O_2/OH^-}. Assuming the $Ni_{0.8}Fe_{0.2}O_xH_y$ layer maintains the same hole-collection efficiency on both types of hematite samples (i.e., that the details of the semiconductor|catalyst interface are similar), the lower degree of catalyst charging for $Ni_{0.8}Fe_{0.2}O_xH_y$ on ED-hematite suggests a significant recombination current through the shunts. We note that in the potential range of $-0.2\ V < V_{sem} < 0.2\ V$ vs ε_{O_2/OH^-} (Figure 4a), this shunt current is not sufficient to completely pin the catalyst potential (V_{WE2}) to the substrate potential V_{sem}; hole injection from the semiconductor is in competition with recombination at the FTO through pinholes. Figure 4a further shows that at higher V_{sem} of >0.2 V vs ε_{O_2/OH^-}, when on ED-hematite, $Ni_{0.8}Fe_{0.2}O_xH_y$ is charged to the same potential in both the light and the dark. This is consistent with the FTO controlling the charge state of the catalyst once the FTO is at a positive potential sufficient to oxidize the catalyst in the absence of photogenerated holes. We further note that none of the above results can be explained by different optical properties and hence carrier generation rates of the ED- and ALD-hematite films; they are of similar thickness based on the TEM crosssection and have been shown previously to have similar optical absorption profiles.[43]

Scheme 1. Schematic Band Structure of α-Fe_2O_3|Ni(Fe)O_xH_y|Au|Solution Architectures[a]

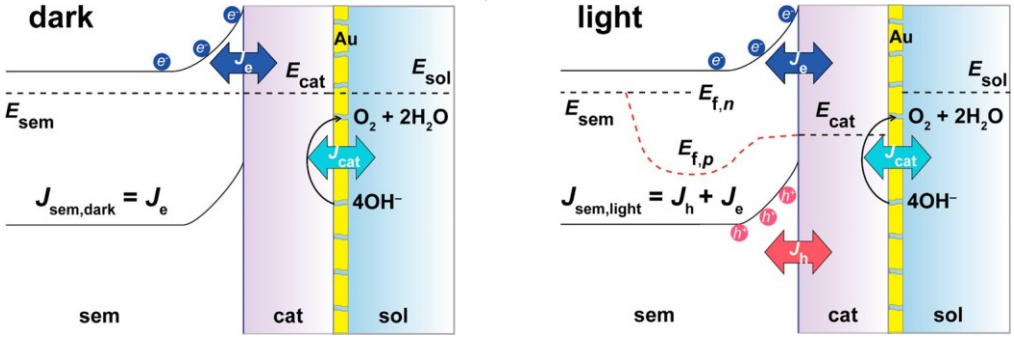

[a] Adapted from ref 18. Copyright 2017 American Chemical Society.

DOI: 10.1021/acsenergylett.8b00336
ACS Energy Lett. 2018, 3, 961–969

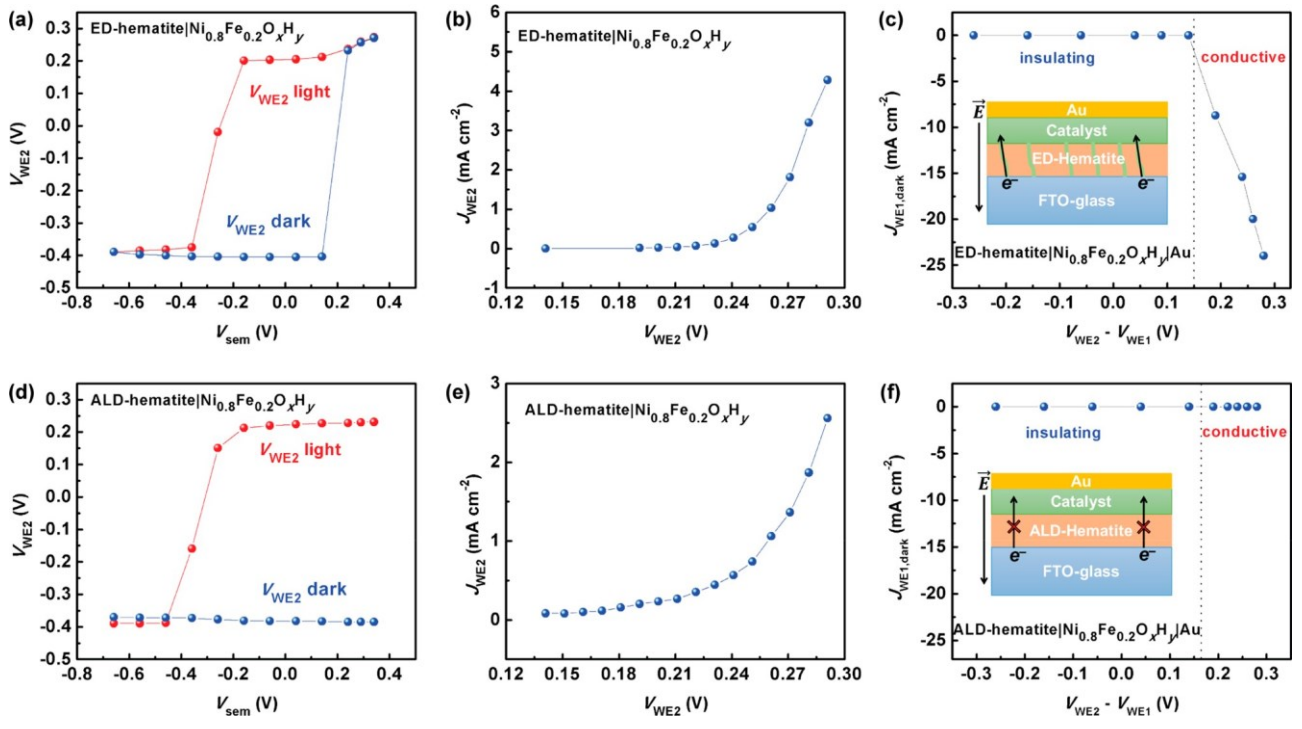

Figure 4. DWE (photo)electrochemical characterization of $Ni_{0.8}Fe_{0.2}O_xH_y$-catalyzed ED-hematite and ALD-hematite. (a) Potentials of the $Ni_{0.8}Fe_{0.2}O_xH_y$ catalyst layer (V_{WE2}) measured from the thin Au working electrode in the dark (blue points) and under one sun illumination (red points) as a function of potential applied to the ED-hematite back contact (V_{sem}). (b) Steady-state current density of $Ni_{0.8}Fe_{0.2}O_xH_y$ layer (on ED-hematite) driving OER in the dark when biased through the top Au WE2. This data shows the OER current passing at the given catalyst potentials in panel a. (c) Current density passing from Au through $Ni_{0.8}Fe_{0.2}O_xH_y$-catalyzed ED-hematite to the FTO substrate when V_{WE1} is held at 0 V vs ε_{O_2/OH^-} and V_{WE2} is set at various potentials. The large currents passing when the catalyst is oxidized to an electronically conducting state are consistent with pinholes in the ED-hematite. (d) Potentials of the $Ni_{0.8}Fe_{0.2}O_xH_y$ catalyst layer (V_{WE2}) in the dark (blue points) and under one sun illumination (red points) as a function of the potential applied to the ALD-hematite (V_{sem}). (e) Steady-state current density of $Ni_{0.8}Fe_{0.2}O_xH_y$ layer (on ALD-hematite) driving OER in the dark when biased through the top Au WE2. This data shows the OER current density passing at the given catalyst potentials in panel d. (f) Current density passing from Au through $Ni_{0.8}Fe_{0.2}O_xH_y$-catalyzed ALDhematite to the FTO substrate when V_{WE1} is held at 0 V vs ε_{O_2/OH^-} and V_{WE2} is set at various potentials. The negligible current flow even when the catalyst is oxidized and conductive is consistent with a continuous pinhole-free ALD-hematite film. The potentials V_{sem}, V_{WE1}, and V_{WE2} are reported vs ε_{O_2/OH^-}.

The dark measurements in Figure 4a,d agree with the above hypothesis. In the absence of photogenerated holes, leakage currents across the junction or through shunt pathways are the only mechanisms to oxidize the catalyst. Figure 4d shows that the $Ni_{0.8}Fe_{0.2}O_xH_y$ layer on ALD-hematite is not oxidized in the dark. However, the $Ni_{0.8}Fe_{0.2}O_xH_y$ layer on ED-hematite is oxidized under anodic potentials (Figure 4a, blue points). This is consistent with catalyst shunting to the FTO substrates for ED-hematite but not for ALD-hematite.

We next measured the current flowing through the catalyst film using the DWE configuration. The potential of hematite was fixed ($V_{WE1} = V_{sem} = 0$ V vs ε_{O_2/OH^-}), and the potential of the $Ni_{0.8}Fe_{0.2}O_xH_y$ catalyst (V_{WE2}) is anodically stepped from the insulating to the conducting regions.

When the catalyst is conductive ($V_{WE2} \geq 0.21$ V vs ε_{O_2/OH^-}), a small potential difference between WE2 and WE1 ($V_{WE2} - V_{WE1}$) is insufficient to result in significant electronic current flow from hematite to $Ni_{0.8}Fe_{0.2}O_xH_y$ because of the Schottky barrier at the hematite|catalyst interface (Scheme 1). As expected, this is the case for ALD-hematite|$Ni_{0.8}Fe_{0.2}O_xH_y$|Au devices (Figures 4f and S3b). However, a large current from the ED-hematite to the conductive $Ni_{0.8}Fe_{0.2}O_xH_y$ is observed (Figures 4c and S3a) once the catalyst is oxidized to the conductive state. This is further evidence that the direct contact between the conductive $Ni_{0.8}Fe_{0.2}O_xH_y$ layer and FTO, observed by TEM, leads to large recombination currents under illumination.

If shunting between the catalyst and substrate causes poor PEC performance for ED-hematite, then the electrical conductivity of the catalyst should affect the nature of the photoresponse. To test this hypothesis, we employ $Ni_{0.2}Fe_{0.8}O_xH_y$, an electrical insulator.[36,38] Its low conductivity may result from phase-segregated insulating Fe oxyhydroxide domains.[36] We find that $Ni_{0.2}Fe_{0.8}O_xH_y$-

DOI: 10.1021/acsenergylett.8b00336
ACS Energy Lett. 2018, 3, 961–969

catalyzed ED-hematite does not show signatures of shunting when measured in the DWE geometry (Figure S4), in contrast to the $Ni_{0.8}Fe_{0.2}O_xH_y$ on ED-hematite discussed above. This data therefore explains why the poor catalyst, $Ni_{0.2}Fe_{0.8}O_xH_y$, is superior to the faster catalyst, $Ni_{0.8}Fe_{0.2}O_xH_y$, only when the possibility of shunting through pinholes exists on the ED sample (compare panels b and c in Figure 2). The data may also explain why high-Fecontent $Ni_{0.5}Fe_{0.5}O_xH_y$ catalysts were used successfully previously to produce high-photovoltage hematite photoelectrodes.[13] Here we find that $Ni_{0.5}Fe_{0.5}O_xH_y$ is also a poor electrical conductor (electrical conductivity of ~10^{-6} mS·cm^{-1} at 0.29 V vs ε_{O2/OH^-}, 4 orders of magnitude lower than that of $Ni_{0.8}Fe_{0.2}O_xH_y$; see Figure S5). Accordingly, the dark current of ED-hematite|$Ni_{0.5}Fe_{0.5}O_xH_y$ is much lower than that of EDhematite|$Ni_{0.8}Fe_{0.2}O_xH_y$ (Figure S5b).

If photogenerated holes are consumed before they charge the catalyst layer to make it conductive, the recombination pathway should also be eliminated. When ED-hematite|$Ni_{0.8}Fe_{0.2}O_xH_y$, a poorly performing photoelectrode, is immersed in alkaline solution with H_2O_2 hole scavenger, the $Ni_{0.8}Fe_{0.2}O_xH_y$ catalyst stays uncharged (and thus nonconductive) as the H_2O_2 rapidly scavenges holes. The photocurrent−potential behavior thus improves dramatically (Figure S6). This is consistent with the hypothesis that the poor performance arises from shunting to the underlying FTO through the conductive catalyst layer.

Selective Catalyst Deposition To Avoid Shunting. The above results suggest that the PEC performance of ED-hematite should be enhanced with a good OER catalyst, if catalyst shunting can be avoided. Thus, for an efficient catalyst contact it is critical that no recombination/charge-transport pathways exist between the catalyst and conductive substrate. To test this hypothesis, we employed a photoassisted anodic deposition (Figure 5a), intended to selectively deposit catalyst on the semiconductor surface via reaction with photogenerated holes (experimental details are included in the Supporting Information). Because holes in the FTO do not experience the photovoltage, and thus do not

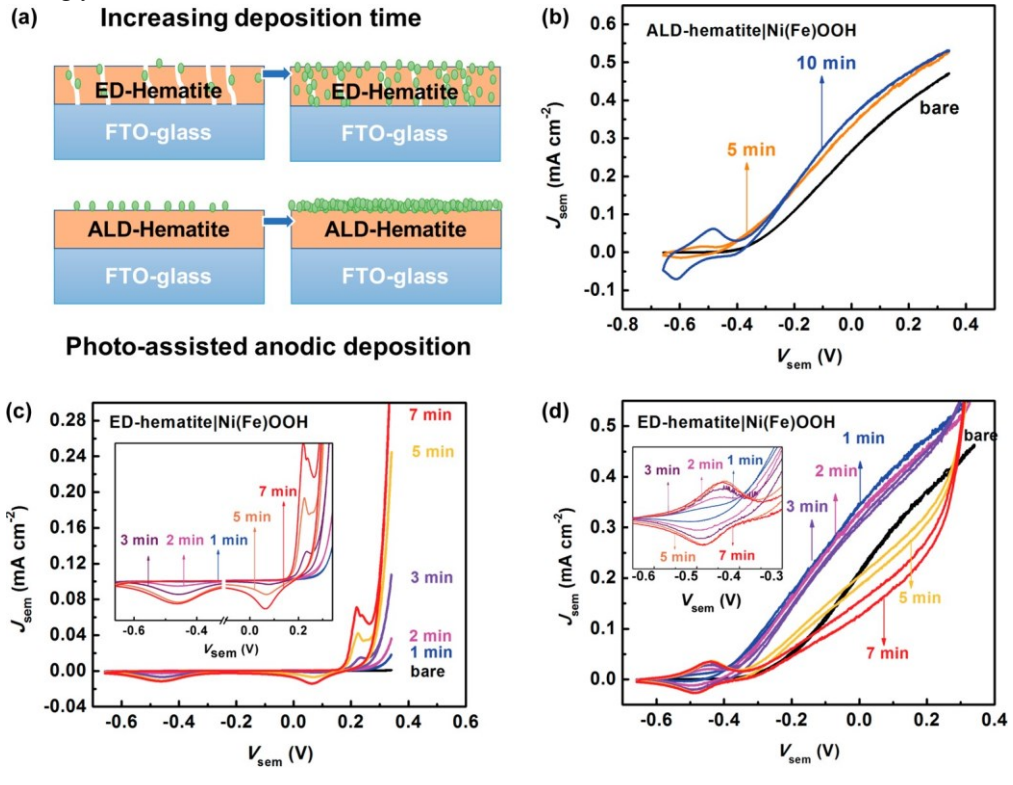

Figure 5. Photoassisted anodic deposition of Ni(Fe)O_xH_y catalyst on hematite electrodes. (a) Schematic showing possible catalyst distribution for low and high loading on ED-hematite and ALD-hematite. (b) Illuminated current voltage curves collected for ALD-hematite samples with different loadings (bare and after 5 and 10 min deposition) of Ni(Fe)O_xH_y. Higher loading results in better performance due to the lack of recombination through pinholes. (c) Dark current densities collected for ED-hematite samples with different loadings of Ni(Fe)O_xH_y on EDhematite. The reversible Ni redox wave at ~0.2 V is attributed to Ni(Fe)O_xH_y in direct contact with the FTO. (d) Photocurrent densities recorded for ED-hematite with different loadings of Ni(Fe)O_xH_y. The decrease in photoresponse with higher loading is attributed to recombination due to direct catalyst-FTO contact, as shown in panel a. Insets in panels c and d more clearly show the Ni redox wave. The potentials V_{sem} are reported vs ε_{O2/OH^-}. The voltammetry data were collected at 10 mV·s^{-1} in 0.1 M KOH. Illuminated data were collected with ~100 mW·cm^{-2} of AM1.5G solar simulation incident on the FTO side of the sample.

DOI: 10.1021/acsenergylett.8b00336
ACS Energy Lett. 2018, 3, 961–969

reach sufficiently oxidizing potentials, this strategy can prevent the catalyst from depositing on exposed FTO.

Photoassisted anodic deposition of Ni(Fe)O_xH_y (NiO_xH_y with unintentional doping of Fe from electrolyte impurities[31]) on ALD-hematite improves its photocurrent and shifts the photocurrent onset cathodic (Figure 5b). Increased loading of Ni(Fe)O_xH_y catalyst (0.38 mC·cm^{-2} in the integrated charge of the Ni reduction peak) results in a larger Ni redox peak and improved PEC performance while dark currents do not increase significantly (Figure S7), in agreement with Hamann and co-workers′ studies, where increasing loading of CoPi via photodeposition on hematite also improves PEC performance.[24] Additionally, unintentional Fe incorporation in the catalyst, which makes Ni(Fe)O_xH_y more catalytically active, led to higher photocurrent (Figure S8). This data thus confirms the conclusion that a high-activity, electrically conductive catalyst is better in the absence of catalyst shunting.

When Ni(Fe)O_xH_y is photoanodically deposited onto EDhematite, the PEC performance initially increased before decreasing at higher loadings (Figure 5d). Photodeposition of Ni(Fe)O_xH_y for 1−3 min leads to the largest improvement (Figure 5d). Superior performance of the thin layers on EDhematite suggests that catalyst-mediated "shunting" recombination is not significantly occurring. Higher loading of Ni(Fe)O_xH_y (5−7 min photodeposition producing 0.25 mC· cm^{-2} in the integrated charge of the Ni reduction peak) leads to lower photocurrent between 0 and 0.3 V vs ε_{O_2/OH^-} (Figure 5d).

The decrease in photocurrent is likely associated with an increasing amount of Ni oxyhydroxide in contact with FTO.

To better understand this phenomenon on ED-hematite, we analyzed the dark current−potential response of the system (Figure 5c). The reduction peak at ∼0.07 V vs ε_{O_2/OH^-} is attributed to the reduction of Ni oxyhydroxide in direct contact with FTO. The reduction peak at ∼−0.47 V vs ε_{O_2/OH^-} is due to Ni oxyhydroxide reduction through the hematite. The shift in redox potential is attributed to the electronic barrier that charge must pass at the hematite|catalyst interface. With increasing photoanodic deposition time (e.g., 5 and 7 min), large redox peaks grow in at ∼0.07 V vs ε_{O_2/OH^-} that are associated with Ni(Fe)O_xH_y in direct contact with the FTO. Similar to Ni(Fe)O_xH_y, when CoPi is photodeposited on EDhematite, an increased then decreased photocurrent is also observed as the deposition amount is increased (Figure S9).

This data may also explain the similar thickness-dependent performance of CoPi modified hematite measured by Carroll et al.[12,44] In these studies, an optimal performance was achieved with thin CoPi (2.5 nm thick), and reduced performance was observed for thicker catalyst layers (25 nm). This observation was attributed to increased recombination of conduction band electrons as they are extracted through the back contact because of the buildup of holes in the thicker catalyst layer.[12] We note, however, that the authors also show substantial dark currents for the thicker catalyst layers, consistent with direct contact of the catalyst with the underlying FTO.

It is useful to also consider the recombination at a more fundamental level. Recombination occurs as majority electrons transfer to acceptor states (i.e., oxidized catalyst sites) in the catalyst via tunneling from the conduction band edge. Tunneling transport decays exponentially with distance and, through solids, is operative for distances typically on the order of ∼1 nm.[45] The recombination rate will then be proportional to the number of acceptor states available (oxidized catalyst per volume) in this thin interface region. However, the number of acceptor sites accessible to charge transfer from the conduction band remains constant after the first 1−2 nm of catalyst layer, i.e., the addition of more catalyst does not increase the number of accessible acceptors. Therefore, it is unlikely that thicker catalyst layers on the order of 25 nm would lead to more recombination by this mechanism. A more plausible explanation for the reduced performance of the thick layers is shunting of catalyst to the FTO back contact, as we provide direct evidence for in the systems studied here. CoPi is also known to be an electrical conductor when oxidized.[46] Similarly, the observation that a thinner Ni (oxy)hydroxide layer does not diminish the photocurrent of hematite nanorods[29] can also be explained by the thin layer limiting the catalyst shunt pathway.

Electrically Blocking Layers. Surface passivation, i.e., presumably the elimination of surface states through deposition of a thin oxide layer, has also been shown to be effective in improving the PEC performance.[47,48] We deposited Al_2O_3 film (thickness ∼1 nm) on the surface of ED-hematite and into any pinholes that may expose the underlying FTO via ALD before spin coating the $Ni_{0.8}Fe_{0.2}O_xH_y$ catalyst film. Figure S10 shows that this ALD-Al_2O_3 layer effectively decreases the dark electronic current; redox features due to direct contact between electrochemically active Ni (oxy)hydroxide and FTO are not observed at ∼0.15 V vs ε_{O_2/OH^-}. The absence of catalyst shunting leads to an increased photocurrent. These results may be relevant to understanding the excellent performance of FeOOH|NiOOH double-layer electrocatalyst on nanoporous $BiVO_4$ photoanodes:[32] the electrically insulating FeOOH layer may help prevent shunting of the NiOOH to the underlying conductive glass.

A Picture of Catalyst Deposition, Shunt Pathways, and System Performance. All the observations here support a simple picture of the semiconductor|catalyst interface where the catalyst collects photogenerated holes from the semiconductor, oxidizing the catalyst and driving the OER current. Higherperformance catalysts, or higher loadings of catalyst, yield higher performance, provided the shunt pathways can be avoided. Although a simple mechanism

DOI: 10.1021/acsenergylett.8b00336
ACS Energy Lett. 2018, 3, 961−969

compared to various interpretations involving surface states and interface recombination,[12,20,21,32,47] recombination through shunts has not been previously considered for these systems. We show that such shunting recombination can be avoided by four different design strategies. (1) A semiconductor film completely covering the underlying conducting oxide, e.g., prepared by ALD, can be used. (2) An electronically insulating catalyst can be used even in the presence of pinholes, although this leads to lower catalyst activity as few of the metal cation sites are electrochemically active (i.e., in electronic communication with the semiconductor). (3) Selective photoassisted anodic deposition of a sufficiently thin catalyst layer on the semiconductor can be used, preventing the catalyst from contacting the underlying FTO. (4) Finally, deposition of a thin insulating layer over the porous semiconductor structure lowers shunting recombination current.

Although not demonstrated here, the work suggests that selectively coating the exposed underlying conductive FTO with an insulator (i.e., plugging the pinholes), while leaving the hematite exposed, would improve performance further. Another high-performance photoelectrode structure might consist of a thin, dense semiconductor film (deposited e.g. by ALD) onto which a high-surface-area nanostructured semiconductor is deposited. This would prevent the possibility of shunting while harnessing the benefit of the high surface area for carrier collection.

ASSOCIATED CONTENT

* Supporting Information

The Supporting Information is available free of charge on the ACS Publications website at DOI: 10.1021/acsenergylett.8b00336.

Experimental methods and additional photoelectrochemical and DWE data (PDF)

AUTHOR INFORMATION

Corresponding Author *E-mail: swb@uoregon.edu.

ORCID

Sebastian Z. Oener: 0000-0003-0770-4089

Thomas W. Hamann: 0000-0001-6917-7494

Shannon W. Boettcher: 0000-0001-8971-9123

Notes

The authors declare no competing financial interest.

ACKNOWLEDGMENTS

This work was funded by the Department of Energy, Basic Energy Sciences, award number DE-SC0014279. S.W.B also acknowledges support from the Sloan and Dreyfus foundations.

H.H. and T.W.H. were responsible for growing the hematite photoelectrodes by ALD and electrodeposition supported by NSF award CHE-1150378, and provided supporting data and insightful comments regarding the data analysis. We acknowledge use of the CAMCOR shared instrumentation, which is supported by grants from the M. J. Murdock Charitable Trust, the W. M. Keck Foundation, ONAMI, and the NSF. We also acknowledge use of the Rapid Materials Prototyping facility, funded by the Murdock Charitable Trust. We thank Robert Fischer and Joshua Razink for assistance with FIB and HRTEM analysis.

REFERENCES

(1) Walter, M. G.; Warren, E. L.; McKone, J. R.; Boettcher, S. W.; Mi, Q. X.; Santori, E. A.; Lewis, N. S. Solar Water Splitting Cells. Chem. Rev. 2010, 110, 6446−6473.

(2) Hunter, B. M.; Gray, H. B.; Muller, A. M. Earth-Abundant Heterogeneous Water Oxidation Catalysts. Chem. Rev. 2016, 116, 14120−14136.

(3) Sivula, K.; van de Krol, R. Semiconducting Materials for Photoelectrochemical Energy Conversion. Nat. Rev. Mater. 2016, 1, 15010.

(4) Yourey, J. E.; Bartlett, B. M. Electrochemical Deposition and Photoelectrochemistry of $CuWO_4$, a Promising Photoanode for Water Oxidation. J. Mater. Chem. 2011, 21, 7651−7660.

(5) Guijarro, N.; Bornoz, P.; Prevot, M.; Yu, X.; Zhu, X.; Johnson, M.; Jeanbourquin, X.; Le Formal, F.; Sivula, K. Evaluating Spinel Ferrites MFe_2O_4 (M = Cu, Mg, Zn) as Photoanodes for Solar Water Oxidation: Prospects and Limitations. Sustainable Energy Fuels 2018, 2, 103−117.

(6) Sivula, K.; Zboril, R.; Le Formal, F.; Robert, R.; Weidenkaff, A.; Tucek, J.; Frydrych, J.; Gratzel, M. Photoelectrochemical Water Splitting with Mesoporous Hematite Prepared by a Solution-Based Colloidal Approach. J. Am. Chem. Soc. 2010, 132, 7436−7444.

(7) Li, M. Y.; Yang, Y.; Ling, Y. C.; Qiu, W. T.; Wang, F. X.; Liu, T. Y.; Song, Y.; Liu, X. X.; Fang, P. P.; Tong, Y. X.; et al. Morphology and Doping Engineering of Sn-Doped Hematite Nanowire Photoanodes. Nano Lett. 2017, 17, 2490−2495.

(8) Gurudayal; Chee, P. M.; Boix, P. P.; Ge, H.; Yanan, F.; Barber, J.; Wong, L. H. Core-Shell Hematite Nanorods: A Simple Method to Improve the Charge Transfer in the Photoanode for Photoelectrochemical Water Splitting. ACS Appl. Mater. Interfaces 2015, 7, 6852−6859.

(9) Peerakiatkhajohn, P.; Yun, J. H.; Chen, H. J.; Lyu, M. Q.; Butburee, T.; Wang, L. Z. Stable Hematite Nanosheet Photoanodes

DOI: 10.1021/acsenergylett.8b00336
ACS Energy Lett. 2018, 3, 961−969

for Enhanced Photoelectrochemical Water Splitting. Adv. Mater. 2016, 28, 6405−6410.
(10) Zhong, D. K.; Gamelin, D. R. Photoelectrochemical Water Oxidation by Cobalt Catalyst ("Co-Pi")/α-Fe_2O_3 Composite Photoanodes: Oxygen Evolution and Resolution of a Kinetic Bottleneck. J. Am. Chem. Soc. 2010, 132, 4202−4207.
(11) Tilley, S. D.; Cornuz, M.; Sivula, K.; Gratzel, M. Light-Induced Water Splitting with Hematite: Improved Nanostructure and Iridium Oxide Catalysis. Angew. Chem., Int. Ed. 2010, 49, 6405−6408.
(12) Carroll, G. M.; Zhong, D. K.; Gamelin, D. R. Mechanistic Insights into Solar Water Oxidation by Cobalt-Phosphate-Modified αFe_2O_3 Photoanodes. Energy Environ. Sci. 2015, 8, 577−584.
(13) Du, C.; Yang, X. G.; Mayer, M. T.; Hoyt, H.; Xie, J.; McMahon, G.; Bischoping, G.; Wang, D. W. Hematite-Based Water Splitting with Low Turn-on Voltages. Angew. Chem., Int. Ed. 2013, 52, 12692− 12695.
(14) Gamelin, D. R. Water Splitting Catalyst or Spectator? Nat. Chem. 2012, 4, 965−967.
(15) Nellist, M. R.; Laskowski, F. A. L.; Lin, F. D.; Mills, T. J.; Boettcher, S. W. Semiconductor-Electrocatalyst Interfaces: Theory, Experiment, and Applications in Photoelectrochemical Water Splitting. Acc. Chem. Res. 2016, 49, 733−740.
(16) Ding, C. M.; Shi, J. Y.; Wang, Z. L.; Li, C. Photoelectrocatalytic Water Splitting: Significance of Cocatalysts, Electrolyte, and Interfaces. ACS Catal. 2017, 7, 675−688.
(17) Peter, L. M.; Wijayantha, K. G. U. Photoelectrochemical Water Splitting at Semiconductor Electrodes: Fundamental Problems and New Perspectives. ChemPhysChem 2014, 15, 1983−1995.
(18) Qiu, J.; Hajibabaei, H.; Nellist, M. R.; Laskowski, F. A. L.; Hamann, T. W.; Boettcher, S. W. Direct in Situ Measurement of Charge Transfer Processes During Photoelectrochemical Water Oxidation on Catalyzed Hematite. ACS Cent. Sci. 2017, 3, 1015−1025.
(19) Jang, J. W.; Du, C.; Ye, Y. F.; Lin, Y. J.; Yao, X. H.; Thorne, J.; Liu, E.; McMahon, G.; Zhu, J. F.; Javey, A.; et al. Enabling Unassisted Solar Water Splitting by Iron Oxide and Silicon. Nat. Commun. 2015, 6, 7447.
(20) Du, C.; Zhang, M.; Jang, J. W.; Liu, Y.; Liu, G. Y.; Wang, D. W. Observation and Alteration of Surface States of Hematite Photoelectrodes. J. Phys. Chem. C 2014, 118, 17054−17059.
(21) Thorne, J. E.; Jang, J. W.; Liu, E. Y.; Wang, D. W. Understanding the Origin of Photoelectrode Performance Enhancement by Probing Surface Kinetics. Chem. Sci. 2016, 7, 3347−3354.
(22) Zachaus, C.; Abdi, F. F.; Peter, L. M.; van de Krol, R. Photocurrent of $BiVO_4$ Is Limited by Surface Recombination, Not Surface Catalysis. Chem. Sci. 2017, 8, 3712−3719.
(23) Barroso, M.; Cowan, A. J.; Pendlebury, S. R.; Gratzel, M.; Klug, D. R.; Durrant, J. R. The Role of Cobalt Phosphate in Enhancing the Photocatalytic Activity of α-Fe_2O_3 toward Water Oxidation. J. Am. Chem. Soc. 2011, 133, 14868−14871.
(24) Xi, L. F.; Wang, F. X.; Schwanke, C.; Abdi, F. F.; Golnak, R.; Fiechter, S.; Ellmer, K.; van de Krol, R.; Lange, K. M. In Situ Structural Study of MnPi-Modified $BiVO_4$ Photoanodes by Soft X-Ray Absorption Spectroscopy. J. Phys. Chem. C 2017, 121, 19668−19676.
(25) Klahr, B.; Gimenez, S.; Fabregat-Santiago, F.; Bisquert, J.; Hamann, T. W. Photoelectrochemical and Impedance Spectroscopic Investigation of Water Oxidation with "Co-Pi"-Coated Hematite Electrodes. J. Am. Chem. Soc. 2012, 134, 16693−16700.
(26) Lin, F. D.; Boettcher, S. W. Adaptive Semiconductor/Electrocatalyst Junctions in Water-Splitting Photoanodes. Nat. Mater. 2014, 13, 81−86.
(27) Nellist, M. R.; Laskowski, F. A. L.; Qiu, J.; Hajibabaei, H.; Sivula, K.; Hamann, T. W.; Boettcher, S. W. Potential-Sensing Electrochemical Atomic Force Microscopy for in Operando Analysis of Electrocatalysis During (Photo)Electrochemical Water Splitting. Nat. Energy 2018, 3, 46−52.
(28) Young, K. M. H.; Hamann, T. W. Enhanced Photocatalytic Water Oxidation Efficiency with $Ni(OH)_2$ Catalysts Deposited on αFe_2O_3 via ALD. Chem. Commun. 2014, 50, 8727−8730.
(29) Wang, G. M.; Ling, Y. C.; Lu, X. H.; Zhai, T.; Qian, F.; Tong, Y. X.; Li, Y. A Mechanistic Study into the Catalytic Effect of $Ni(OH)_2$ on Hematite for Photoelectrochemical Water Oxidation. Nanoscale 2013, 5, 4129−4133.
(30) Hajibabaei, H.; Schon, A. R.; Hamann, T. W. Interface Control of Photoelectrochemical Water Oxidation Performance with $Ni_{1-x}Fe_xO_y$ Modified Hematite Photoanodes. Chem. Mater. 2017, 29, 6674−6683.
(31) Trotochaud, L.; Young, S. L.; Ranney, J. K.; Boettcher, S. W. Nickel-Iron Oxyhydroxide Oxygen-Evolution Electrocatalysts: The Role of Intentional and Incidental Iron Incorporation. J. Am. Chem. Soc. 2014, 136, 6744−6753.
(32) Kim, T. W.; Choi, K. S. Nanoporous $BiVO_4$ Photoanodes with Dual-Layer Oxygen Evolution Catalysts for Solar Water Splitting. Science 2014, 343, 990−994.
(33) Corrigan, D. A. The Catalysis of the Oxygen Evolution Reaction by Iron Impurities in Thin-Film Nickel-Oxide Electrodes. J. Electrochem. Soc. 1987, 134, 377−384.
(34) Klaus, S.; Cai, Y.; Louie, M. W.; Trotochaud, L.; Bell, A. T. Effects of Fe Electrolyte Impurities on $Ni(OH)_2$/NiOOH Structure and Oxygen Evolution Activity. J. Phys. Chem. C 2015, 119, 7243− 7254.
(35) Stevens, M. B.; Trang, C. D. M.; Enman, L. J.; Deng, J.; Boettcher, S. W. Reactive Fe-Sites in Ni/Fe (Oxy)Hydroxide Are Responsible for Exceptional Oxygen Electrocatalysis Activity. J. Am. Chem. Soc. 2017, 139, 11361−11364.
(36) Friebel, D.; Louie, M. W.; Bajdich, M.; Sanwald, K. E.; Cai, Y.; Wise, A. M.; Cheng, M. J.; Sokaras, D.; Weng, T. C.; Alonso-Mori, R.; et al. Identification of Highly Active Fe Sites in (Ni,Fe)OOH for Electrocatalytic Water Splitting. J. Am. Chem. Soc. 2015, 137, 1305− 1313.
(37) Gorlin, M.; Chernev, P.; Ferreira de Araujo, J.; Reier, T.; Dresp, S.; Paul, B.; Krahnert, R.; Dau, H.; Strasser, P. Oxygen Evolution Reaction Dynamics, Faradaic Charge Efficiency, and the Active Metal Redox States of Ni-Fe Oxide Water Splitting Electrocatalysts. J. Am. Chem. Soc. 2016, 138, 5603−5614.
(38) Zou, S. H.; Burke, M. S.; Kast, M. G.; Fan, J.; Danilovic, N.; Boettcher, S. W. Fe (Oxy)Hydroxide Oxygen Evolution Reaction Electrocatalysis: Intrinsic Activity and the Roles of Electrical Conductivity, Substrate, and Dissolution. Chem. Mater. 2015, 27, 8011−8020.
(39) Burke, M. S.; Kast, M. G.; Trotochaud, L.; Smith, A. M.; Boettcher, S. W. Cobalt-Iron (Oxy)Hydroxide Oxygen Evolution

DOI: 10.1021/acsenergylett.8b00336
ACS Energy Lett. 2018, 3, 961−969

Electrocatalysts: The Role of Structure and Composition on Activity, Stability, and Mechanism. J. Am. Chem. Soc. 2015, 137, 3638−3648.

(40) Smith, R. D. L.; Prevot, M. S.; Fagan, R. D.; Zhang, Z. P.; Sedach, P. A.; Siu, M. K. J.; Trudel, S.; Berlinguette, C. P. Photochemical Route for Accessing Amorphous Metal Oxide Materials for Water Oxidation Catalysis. Science 2013, 340, 60−63.

(41) Natan, M. J.; Belanger, D.; Carpenter, M. K.; Wrighton, M. S. pH-Sensitive $Ni(OH)_2$-Based Microelectrochemical Transistors. J. Phys. Chem. 1987, 91, 1834−1842.

(42) Klahr, B. M.; Martinson, A. B. F.; Hamann, T. W. Photoelectrochemical Investigation of Ultrathin Film Iron Oxide Solar Cells Prepared by Atomic Layer Deposition. Langmuir 2011, 27, 461−468.

(43) Zandi, O.; Schon, A. R.; Hajibabaei, H.; Hamann, T. W. Enhanced Charge Separation and Collection in High-Performance Electrodeposited Hematite Films. Chem. Mater. 2016, 28, 765−771.

(44) Carroll, G. M.; Gamelin, D. R. Kinetic Analysis of Photoelectrochemical Water Oxidation by Mesostructured Co-Pi/α-Fe_2O_3 Photoanodes. J. Mater. Chem. A 2016, 4, 2986−2994.

(45) Smalley, J. F.; Feldberg, S. W.; Chidsey, C. E. D.; Linford, M. R.; Newton, M. D.; Liu, Y. P. The Kinetics of Electron-Transfer Through Ferrocene-Terminated Alkanethiol Monolayers on Gold. J. Phys. Chem. 1995, 99, 13141−13149.

(46) Costentin, C.; Porter, T. R.; Saveant, J. M. Conduction and Reactivity in Heterogeneous-Molecular Catalysis: New Insights in Water Oxidation Catalysis by Phosphate Cobalt Oxide Films. J. Am. Chem. Soc. 2016, 138, 5615−5622.

(47) Le Formal, F.; Tetreault, N.; Cornuz, M.; Moehl, T.; Gratzel, M.; Sivula, K. Passivating Surface States on Water Splitting Hematite Photoanodes with Alumina Overlayers. Chem. Sci. 2011, 2, 737−743.

(48) Eisenberg, D.; Ahn, H. S.; Bard, A. J. Enhanced Photoelectrochemical Water Oxidation on Bismuth Vanadate by Electrodeposition of Amorphous Titanium Dioxide. J. Am. Chem. Soc. 2014, 136, 14011−14014.

DOI: 10.1021/acsenergylett.8b00336
ACS Energy Lett. 2018, 3, 961−969